

Modelling the thermal behaviour of Ti6Al4V sintered powder bed in electron beam powder bed fusion (EB-PBF)

Original

Modelling the thermal behaviour of Ti6Al4V sintered powder bed in electron beam powder bed fusion (EB-PBF) / Galati, Manuela; Campagnoli, Elena; Giarretto, Valter; Iuliano, Luca. - 118:(2023), pp. 664-669. (Intervento presentato al convegno 16th CIRP Conference on Intelligent Computation in Manufacturing Engineering) [10.1016/j.procir.2023.06.114].

Availability:

This version is available at: 11583/2980837 since: 2023-08-01T13:18:34Z

Publisher:

Elsevier

Published

DOI:10.1016/j.procir.2023.06.114

Terms of use:

This article is made available under terms and conditions as specified in the corresponding bibliographic description in the repository

Publisher copyright

(Article begins on next page)

16th CIRP Conference on Intelligent Computation in Manufacturing Engineering, CIRP ICME '22, Italy

Modelling the thermal behaviour of Ti6Al4V sintered powder bed in electron beam powder bed fusion (EB-PBF)

Manuela Galati^{a,*}, Elena Campagnoli^b, Valter Giaretto^b, Luca Iuliano^a

^aDepartment of Management and Production Engineering, Politecnico di Torino, Torino, 10129, Italy

^bDepartment of Energy, Politecnico di Torino, Torino, 10129, Italy

* Corresponding author. Tel.: +390110904569; E-mail address: manuela.galati@polito.it

Abstract

The understanding of thermal behaviour of the sintered powder is a crucial feature in the electron beam powder bed fusion (EB-PBF) process. Accurate analyses may help optimise the process, manage smoke sensitivity materials, and give precious inputs for EB-PBF process modelling and simulation. The major issue in obtaining such kind of information is related to the working conditions of EB-PBF: high temperature and vacuum environment. Moreover, the powder bed should be considered a porous material. Using ad-hoc designed samples and experiments, this work presents an analysis of the thermal behaviour of the Ti6Al4V sintered powder in the EB-PBF process. An experimental campaign has been carried out to evaluate the variation of thermal conductivity of Ti6Al4V sintered powder with the powder thickness and the temperature up to 800°C, which corresponds to the common working temperature for processing Ti6Al4V by EB-PBF.

© 2023 The Authors. Published by Elsevier B.V.

This is an open access article under the CC BY-NC-ND license (<https://creativecommons.org/licenses/by-nc-nd/4.0>)

Peer-review under responsibility of the scientific committee of the 16th CIRP Conference on Intelligent Computation in Manufacturing Engineering

Keywords: Electron beam powder bed fusion; Thermal conductivity; Ti6Al4V; Sintering

1. Introduction

Additive manufacturing (AM) processes are becoming state of the art in the manufacturing sector, especially for metallic components. The most common AM processes for metallic parts are based on the powder bed, which can be melted by either using a laser or an electron beam [1]. Additionally, in the case of electron beam powder bed fusion (EB-PBF), before proceeding with the melting, the entire powder bed is preheated to create small connections among the particles and a slight level of sintering which enhances the thermal conductivity of the powder and reduces the thermal gradient between the melted area and the surrounding [2]. All the process occurs in vacuum [3].

To increase the reliability of AM processes, efforts have been dedicated to modelling and simulation. In this field, the most diffuse models are based on the use of finite element (FE) and homogenised properties [1,4]. Because of that, the proper

set of the input in terms of temperature-dependent material properties from a macroscopic point of view becomes crucial [4].

Chief among these properties is the thermal conductivity [5]. The bulk material can be considered fully described in the literature [6]. However, experimental data on the thermal conductivity of powder are still limited [5]. Analytical models have been proposed to forecast the thermal conductivity of powders [7]. However, some of them fail to incorporate the heat transfer due to the radiation occurring in the empty spaces between the particles. Others considered a specific powder particles arrangement and uniform powder size, e.g. Ref. [8,9]. Many of them considered parameters challenging to be evaluated at different temperatures. Numerical models have been implemented to analyse the heat transfer in the powder bed. As an example, Grose et al. [10] used a phase-field (PF) model to emulate the sintering among copper nanoparticles

during a micro selective laser sintering process. These results have been then used as input for a FE model to analyse the heat transfer through the particles sintered at different temperatures. The coupling between PF and FE was required to analyse phenomena occurring at different process scales. Experimentally, an increasing amount of effort has been devoted to evaluating thermal conductivity. Wei et al. [11] measured the thermal conductivity of loose powder using the hot wire method. Zhang et al. [12] produced a Ti6Al4V hollowed sample by laser powder bed fusion (L-PBF) in which the internal hole was cone-shaped. To obtain the thermal conductivity was then necessary to combine multiple analysis techniques such as laser flash, FE heat transfer modelling and a multivariate inverse method. The obtained results showed a thermal conductivity between 3.4% and 5.2% of the corresponding bulk material. Gong et al. [13] reported thermal conductivity of powder for EB-PBF varying from 2.7 W/m×K at 25°C to 4.0 W/m×K at 750 °C measured by a T2500S thermal analyser. The used specimen was a squared hollowed sample with an edge of 40 mm, a shell of 2.54 mm and 13 mm in height. However, the experimental part was not fully described, specifically how the presence of multiple materials was considered during the measurements. Laser flash measurements were used by Neira Arce [14] and Smith et al. [8] to measure the thermal conductivity of EB-PBF powders at different temperatures. Neira Arce [14] used a sample of loose powder, while Smith et al. [15] used samples of sintered powder. Leung et al. [16] evaluated the thermal conductivity of sintered powder at room temperature using heat flux simulation starting from a tomogram in which the connections between the particles were visible [17]. While these results can be valuable to model techniques such as L-PBF, the high level of sintering and the presence of vacuum for EB-PBF make those literature data insufficient to represent the EB-PBF process adequately. Particularly, the variation of processing temperature in a wide range, the powder sintering state, and the presence of vacuum in the chamber should be taken into account.

This work investigates the thermal conductivity experimentally using an ad-hoc designed sample. The sample consists of a hollowed shelled disk containing powder sintered during the process. The laser flash method was used to measure the thermal diffusivity and the thermal conductivity of the samples. Then, mathematical models are used to extract the thermal conductivity of the powder layer only. Moreover, the effect of the powder thickness on the thermal properties is also analysed.

2. Material and method

Fig. 1 depicts the CAD sample design, consisting of a hollowed disk with an external diameter of 9.79 mm and 4 mm thick. The internal hole is circular, and its diameter is 8.49 mm. Therefore, the shell around the sintered powder was equal to 0.5 mm. The hole thickness was varied between 1.2 mm and 2 mm with a step of 0.2 mm and named S12, S14, S16, S18 and S20, respectively. The specimens were produced using an Arcam A2X and standard Arcam Ti6Al4V powder with a size range between 45µm and 105 µm and standard process parameters [18]. The corresponding preheating temperature on the powder

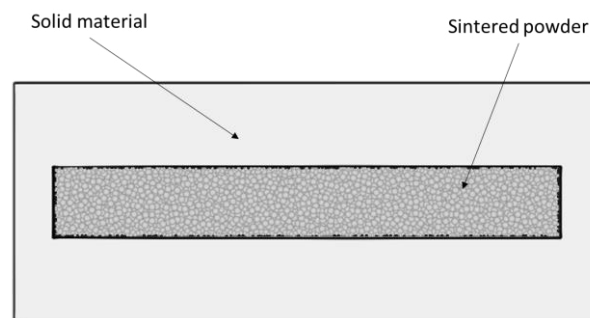


Fig. 1. Cross-section of the sample enclosed a certain thickness of sintered powder.

bed was around 650 °C. The layer thickness was set equal to 0.05 mm. After the production, each disc has been removed from the base, and the circular surface has been uniformly polished up to a total thickness equal to about 3 mm.

The experimental setup and the technique for measuring the thermal properties were based on the laser-flash method [19–21], typically used to measure the thermal diffusivity of multilayer materials [22–26]. The laser pulse is absorbed by the front surface of the sample, while the resulting temperature rise is measured on the rear face using a K type thermocouple (Chromel and Alumel). The two wires of the thermocouple are electrically soldered (the circuit, therefore, closes through the sample) in two different positions around the axis of the sample (a few millimetres apart) to measure the actual average temperature of this central area. For each sample, the chamber temperature was gradually increased until reaching the desired set point, waiting for its stabilization before carrying out the measurements. The measurements have been performed from room temperature up to 800 °C. Specifically, a confirmation experiment has been performed at 400°C using the samples S18 and S20.

Owing to the multi-material nature of the specimens, the determination of properties such as the thermal conductivity (λ), the volumetric heat capacity (ρc , product between the material density ρ and the specific heat c) and the thermal diffusivity α ($\lambda/\rho c$), required specific modelling. The solutions of the heat diffusion equation can be determined using the method reported in Ref. [23]. The equation was solved under the following hypotheses: 1) the heat flux is one-dimensional and passes through homogeneous layers; 2) the laser heat pulse is absorbed uniformly on the front surface of the sample, and there are heat losses from the front and rear surfaces of the sample, which are facing towards the measuring chamber. The effects of thermal contact resistance between the inner and outer layers were not considered to determine the thermal diffusion properties of the sintered powder.

2.1. Mathematical modelling

Assuming that the energy release associated with the laser pulse on the front surface of the sample is instantaneous; the temperature trend close to the sample axis is well described by the following set of equations [27] which must be solved with the appropriate boundary and initial conditions:

$$\frac{\partial^2 \vartheta_j(x,t)}{\partial x^2} = \frac{1}{a_j(T_0)} \frac{\partial \vartheta_j}{\partial t}, \quad j = 1, 2, 3 \quad (1)$$

In the equation the temperature increase $\vartheta_j(x, t)$ is given by the difference between the local temperature $T_j(x, t)$ inside the sample and the constant value T_0 of the measuring chamber, and $a_j(T_0)$ is the thermal diffusivity of the j th layer at the temperature T_0 . The thermal diffusion properties are assumed independent of the temperature increase $\vartheta_j(x, t)$. The initial condition imposed is:

$$\vartheta_j(x, 0) = 0 \quad (2)$$

and the boundary conditions are:

$$-\lambda_1(T_0) \frac{\partial \vartheta_1(x_1, t)}{\partial x} = q\delta(0) - \alpha_1(T_0)\vartheta_1(x_1, t) \quad (3)$$

$$\vartheta_1(0, t) = \vartheta_2(0, t) \quad (4)$$

$$\lambda_1(T_0) \frac{\partial \vartheta_1(0, t)}{\partial x} = \lambda_2(T_0) \frac{\partial \vartheta_2(0, t)}{\partial x} \quad (5)$$

$$\vartheta_2(x_2, t) = \vartheta_3(x_2, t) \quad (6)$$

$$\lambda_2(T_0) \frac{\partial \vartheta_2(x_2, t)}{\partial x} = \lambda_3(T_0) \frac{\partial \vartheta_3(x_2, t)}{\partial x} \quad (7)$$

$$-\lambda_3(T_0) \frac{\partial \vartheta_3(x_3, t)}{\partial x} = \alpha_3(T_0)\vartheta_3(x_3, t) \quad (8)$$

where q is the amount of the energy released by the laser and absorbed by the sample, $\delta(0)$ is the delta function assigned to the laser pulse versus time, while $\lambda_j(T_0)$ is the thermal conductivity of the j th layer, which is determined at the reference temperature T_0 of the test chamber. As suggested and verified in the literature [9], the radiative exchanges between the sample and the surfaces of the test vacuum chamber were linearised, and $\alpha_1(T_0)$ and $\alpha_3(T_0)$ are the heat transfer coefficients valued as:

$$\alpha_1(T_0) = 4\sigma\varepsilon_1 T_0^3 \text{ and } \alpha_3(T_0) = 4\sigma\varepsilon_3 T_0^3 \quad (9)$$

where σ is the Stefan Boltzmann constant and $\varepsilon_1, \varepsilon_3$ are the emissivity of the front and rear surface, respectively assumed independent of the temperature.

Using the hypotheses mentioned above and the initial and boundary conditions reported in Eq. 2 to 8, Eq. (1) can be solved using the Laplace transform technique and the inversion integral proposed by Sweet [23].

In this case, the investigated material is enclosed between two layers of known thickness and the same material and, therefore, with the same thermophysical properties. Therefore, assigning to the external layers a thermal conductivity equal to $\lambda_0 = \lambda_1 = \lambda_3$, a thermal diffusivity $a_0 = a_1 = a_3$, a thermal effusivity $e_0 = e_1 = e_3$ and a thickness $L_0 = L_1 = L_3$, the rear face temperature is given by:

$$\vartheta_3(x_3, t) = q \frac{8a_0}{\lambda_0 L_0} \sum_{k=1}^{\infty} D_k^{-1} \exp\left(-\mu_k^2 \frac{a_0}{L_0^2} t\right) \quad (10)$$

where the term D_k can be expressed as

$$D_k = \psi_1 \chi_1 \cos(\psi_1 \mu_k) + 2\psi_2 \chi_2 \cos(\psi_2 \mu_k) + \psi_3 \chi_3 \cos(\psi_3 \mu_k) + \frac{\beta_1 + \beta_3}{\mu_k^2} \{ \chi_1 [\cos(\psi_1 \mu_k) + \psi_1 \mu_k \sin(\psi_1 \mu_k)] + \chi_3 [\cos(\psi_3 \mu_k) + \psi_3 \mu_k \sin(\psi_3 \mu_k)] \} + \frac{2}{3} \beta_1 \beta_3 \{ 2[\chi_1 \sin(\psi_1 \mu_k) - 2\chi_2 \sin(\psi_2 \mu_k) + \chi_3 \sin(\psi_3 \mu_k)] - \mu_k [\psi_1 \chi_1 \cos(\psi_1 \mu_k) + \psi_3 \chi_3 \cos(\psi_3 \mu_k)] \} \quad (11)$$

in which β_1 and β_3 are equivalent to the Biot numbers written for the external layers as

$$\beta_1 = \frac{\alpha_1 L_0}{\lambda_0} \text{ and } \beta_3 = \frac{\alpha_3 L_0}{\lambda_0} \quad (12)$$

and

$$\chi_1 = 2 + \frac{e_0}{e_2} + \frac{e_2}{e_0} \quad \chi_2 = \frac{e_2}{e_0} - \frac{e_0}{e_2} \quad \chi_3 = 2 - \frac{e_0}{e_2} - \frac{e_2}{e_0} \quad \psi_1 = 2 + \frac{L_2}{L_0} \sqrt{\frac{a_0}{a_2}} \quad \psi_2 = \frac{L_2}{L_0} \sqrt{\frac{a_0}{a_2}} \quad \psi_3 = 2 - \frac{L_2}{L_0} \sqrt{\frac{a_0}{a_2}} \quad (13)$$

while the characteristic equation to identify the eigenvalue μ_k is

$$\chi_1 \sin(\psi_1 \mu_k) + 2\chi_2 \sin(\psi_2 \mu_k) + \chi_3 \sin(\psi_3 \mu_k) - \left\{ \frac{\beta_1 + \beta_3}{\mu_k} [\chi_1 \cos(\psi_1 \mu_k) + \chi_3 \cos(\psi_3 \mu_k)] + \frac{\beta_1 \beta_3}{\mu_k^2} [\chi_1 \sin(\psi_1 \mu_k) - 2\chi_2 \sin(\psi_2 \mu_k) + \chi_3 \sin(\psi_3 \mu_k)] \right\} = 0 \quad (14)$$

2.2. Parameters estimation

According to the hypotheses, Eq. 10 represents the thermal response of the sample, in which the parameters related to the powder are unknown. The parameters are the thermal diffusivity a_2 , the thermal effusivity e_2 , and the laser energy per unit area q , which is absorbed by the sample. Therefore, we can set $\vartheta_3(x_3, t) \equiv \theta(a_2, e_2, q; t)$.

By assigning a set \mathbf{p} of values to the three unknown parameters a_2, e_2 and q , using the model of Eq. 10, it is possible to obtain a calculated vector of temperature increase $\Theta(\mathbf{p})$. Writing these $(N \times 1)$ vectors as

$$\mathbf{M} = \begin{bmatrix} (T_3 - T_0)(t_1) \\ \vdots \\ (T_3 - T_0)(t_N) \end{bmatrix} \text{ and } \Theta(\mathbf{p}) = \begin{bmatrix} \theta(a_2, e_2, q; t_1) \\ \vdots \\ \theta(a_2, e_2, q; t_N) \end{bmatrix} \quad (15)$$

In the case of a model that is non-linearly dependent on the parameters to be estimated, there are few known strategies to obtain the best possible estimate of these unknown parameters and therefore to minimise the difference between the measured temperature increase and that calculated through the model. In this case, no a priori information on unknown parameters was taken into consideration, and therefore the maximum likelihood approach was adopted to minimise the following square function.

$$[\mathbf{M} - \Theta(\mathbf{p})]^T \mathbf{W} [\mathbf{M} - \Theta(\mathbf{p})] = \min \quad (16)$$

where \mathbf{W} is a square weighting matrix $(N \times N)$ relative to the inverse of the covariance matrix of the measurement errors. To minimize the function in Eq. (16) the Gauss-Newton linearization method was applied. Leaving aside the necessary algebra (see for example Ref. 10), a recursive algorithm was implemented, such that the increment at the $i + 1$ iteration for the unknown parameters (3×1) vector $\Delta \mathbf{p}^{(i+1)}$ is given by

$$\Delta \mathbf{p}^{(i+1)} = \mathbf{P}^i \{ \mathbf{X}^T(i) \mathbf{W} [\mathbf{M} - \Theta(\mathbf{p})] \} \quad (17)$$

where \mathbf{X} is the sensitivity $(N \times 3)$ matrix and \mathbf{P} the covariance square (3×3) matrix of the estimated parameters \mathbf{p} . Convergence is achieved when the norm of the vector $\Delta \mathbf{p}^{(i+1)}$ is less of a given imposed value, in our case 10^{-5} .

The vector $\Theta^{(i)}(\mathbf{p})$ is determined at each iteration i assigning the values of the parameters obtained at the previous iteration

$$\Theta^{(i)}(\mathbf{p}) = \begin{bmatrix} \theta(a_2^{(i)}, e_2^{(i)}, q^{(i)}; t_1) \\ \vdots \\ \theta(a_2^{(i)}, e_2^{(i)}, q^{(i)}; t_N) \end{bmatrix} \quad (18)$$

while the matrix \mathbf{P} is related to the sensitivity matrix \mathbf{X} , defined as

$$\mathbf{P}^i = [\mathbf{X}^{T(i)}\mathbf{W}\mathbf{X}^{(i)}]^{-1} \tag{19}$$

$$\mathbf{X}^{(i)} = \begin{bmatrix} \frac{\partial\theta(a_2^{(i)},e_2^{(i)},q^{(i)};t_1)}{\partial a_2^{(i)}} & \frac{\partial\theta(a_2^{(i)},e_2^{(i)},q^{(i)};t_1)}{\partial e_2^{(i)}} & \frac{\partial\theta(a_2^{(i)},e_2^{(i)},q^{(i)};t_1)}{\partial q^{(i)}} \\ \vdots & \vdots & \vdots \\ \frac{\partial\theta(a_2^{(i)},e_2^{(i)},q^{(i)};t_N)}{\partial a_2^{(i)}} & \frac{\partial\theta(a_2^{(i)},e_2^{(i)},q^{(i)};t_1)}{\partial e_2^{(i)}} & \frac{\partial\theta(a_2^{(i)},e_2^{(i)},q^{(i)};t_1)}{\partial q^{(i)}} \end{bmatrix} \tag{20}$$

Note that the partial derivatives representing the coefficients of the previous matrix were obtained numerically, adopting a first-order approximation.

The sensitivity matrix plays a fundamental role in the parameter estimation process, in particular for the identifiability of the parameters. In fact, considering Eq. (19), for the inversion of the matrix \mathbf{P} at each iteration, the following determinant must not be zero

$$|\mathbf{X}^{T(i)}\mathbf{W}\mathbf{X}^{(i)}| \neq \mathbf{0} \tag{21}$$

Obviously, in the case of linearly dependent parameters, this same determinant is formally null.

The matrix \mathbf{P} also depends on the temperature measurement error via the weighting matrix \mathbf{W} . If we assume that these errors are normally distributed, are constant and uncorrelated, then the matrix \mathbf{W} becomes diagonal and proportional to the identity matrix \mathbf{I} through the reciprocal of the variance of the measurement errors. Therefore, to reduce the numerical instabilities that cause a lack of identifiability - i.e. the determinant of Eq. (20) close to zero - the covariance matrix of the estimated parameters was obtained by imposing $\mathbf{W} = \mathbf{I}$ during the iterative process. The uncertainty on the estimated parameters was determined a posteriori (once convergence was reached), assigning to the numerical value of the parameters a confidence interval evaluated both based on the estimated standard deviation and of the bilateral t-distribution for a confidence level of 95% and considering N measurements for each experimental test (typically, $N > 100$).

Once convergence was reached, the standard deviation of the three estimated parameters was obtained from the norm (Euclidean) of the residues $\boldsymbol{\theta}(\mathbf{p}) - \mathbf{M}$ and the main diagonal of the matrix \mathbf{P} , as

$$\sigma_j = \|\boldsymbol{\theta}(\mathbf{p}) - \mathbf{M}\| \sqrt{P_{jj}}, \quad j = 1, 2, 3 \tag{22}$$

In addition to the estimated thermal diffusivity a_2 of the central layer, both the thermal conductivity λ_2 and the volumetric heat capacity $(\rho c)_2$ can be determined through the estimated thermal effusivity e_2 as follows:

$$\lambda_2 = e_2 \sqrt{a_2} = \sqrt{\lambda_2(\rho c)_2} \sqrt{\frac{\lambda_2}{(\rho c)_2}} \quad \text{and} \quad (\rho c)_2 = \frac{e_2}{\sqrt{a_2}} = \frac{\sqrt{\lambda_2(\rho c)_2}}{\sqrt{\frac{\lambda_2}{(\rho c)_2}}} \tag{23}$$

Consequently, the standard deviation of these quantities can be related to the estimated standard deviations σ_{a_2} and σ_{e_2} of a_2 and e_2 , resulting simply

$$\sigma_{\lambda_2} = \frac{\lambda_2}{e_2} t_{95\%} \sigma_{e_2} + \frac{1}{2} \frac{\lambda_2}{a_2} t_{95\%} \sigma_{a_2} \quad \text{and} \quad \sigma_{(\rho c)_2} = \frac{(\rho c)_2}{e_2} t_{95\%} \sigma_{e_2} + \frac{1}{2} \frac{(\rho c)_2}{a_2} t_{95\%} \sigma_{a_2} \tag{24}$$

3. Results and discussion

The thermal diffusivity was measured on bulk samples of the same dimensions and using the same experimental testing, using the classic method suggested by Parker [19].

Within the same temperature range, a linear trend was found for both properties, so that at the temperature $T_{ref} = 20$ °C the following reference values and the temperature coefficients are obtained:

$$\lambda_0(T) = \lambda_{ref} [1 + b_\lambda (T - T_{ref})] \quad \text{with} \quad \lambda_{ref} = 4.29451 \text{ W/(m}\times\text{K)} \text{ and } b_\lambda = 0.002736 \text{ K}^{-1} \tag{25}$$

$$a_0(T) = a_{ref} [1 + b_a (T - T_{ref})] \quad \text{with} \quad a_{ref} = 0.01747 \text{ cm}^2/\text{s} \text{ and } b_a = 0.001460 \text{ 1/K} \tag{26}$$

To consider the radiative losses, the emissivity ε_1 and ε_3 , relative to the front and rear surface of the tri-layers were assumed to be the same.

The emissivity of the surfaces was considered independent of both temperature and wavelength. The assumed emissivity value is 0.3 as reported in the literature for polished Ti-6Al-4V [28].

Fig. 2 shows the thermal diffusivity of sintered powder as the temperature varies. Overall, the thermal diffusivity increases linearly by increasing the temperature. No systematic differences can be observed among the different sintered powder thicknesses. The maximum deviation of the measurements was detected at the highest temperatures. This indicates an inadequacy of the instrument in providing reliable information at high temperatures. The thermal diffusivity varied between 0.005 cm²/s and 0.010 cm²/s. The thermal diffusivity of the samples used as confirmation run at 400°C lies on the estimated line.

Fig. 3 shows the thermal conductivity of the sintered powder at different temperatures compared with the model adopted by Galati et al. [9] in their numerical modelling, where a BCC arrangement of the powder particles was considered. The thermal conductivity varies significantly with the temperature, while no systematic effect can be found for the thickness of the powder layer. The calculated values for the thermal conductivity range between 0.75 W/(m×K) to around 2 W/(m×K). According to the previous results, the highest deviations were observed for the highest temperatures. According to the literature, e.g. Ref. [29], the thermal conductivity of sintered powder is much lower than the corresponding bulk material. The obtained values are higher than the literature data on sintered powder. This difference can be explained by considering many factors including how the powder has been sintered (e.g. density of the powder bed, thermal history) particle size and shape [30].

This result demonstrated the importance of considering the actual processing conditions.

Compared to the analytical model to calculate the thermal conductivity of the powder bed in vacuum proposed by Tolochko et al. [31] and applied to Ti6Al4V in Ref. [9], the measured values are in extremely good agreement.

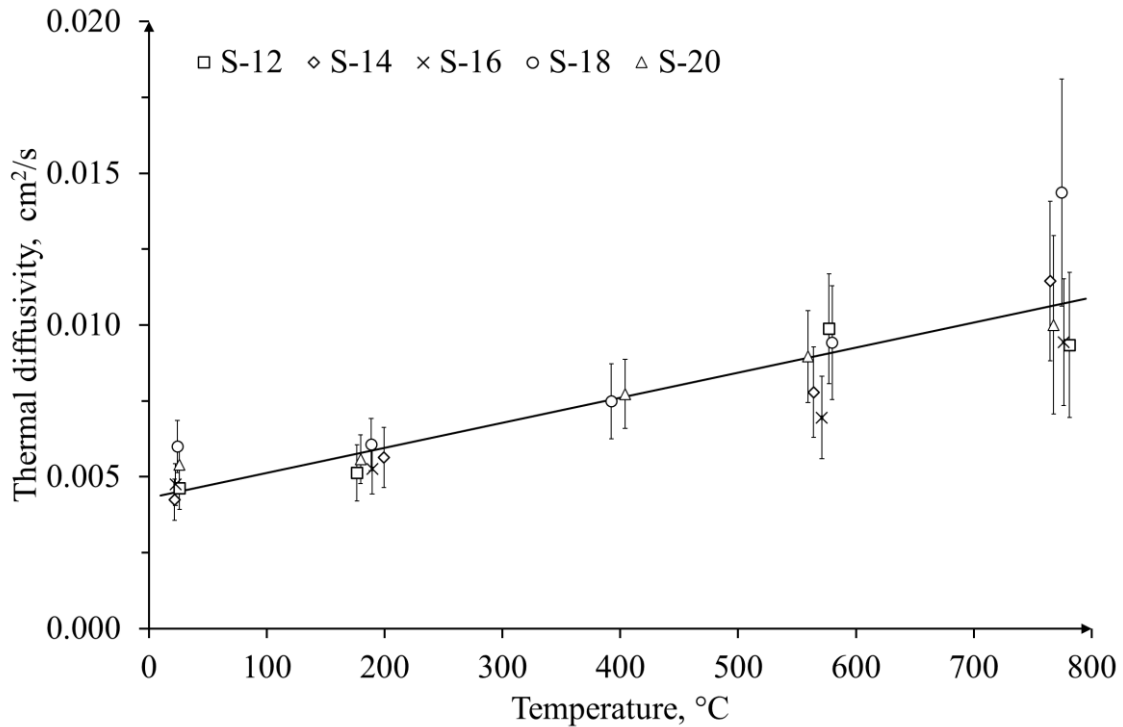


Fig. 2. Thermal diffusivity of sintered Ti6Al4V powder.

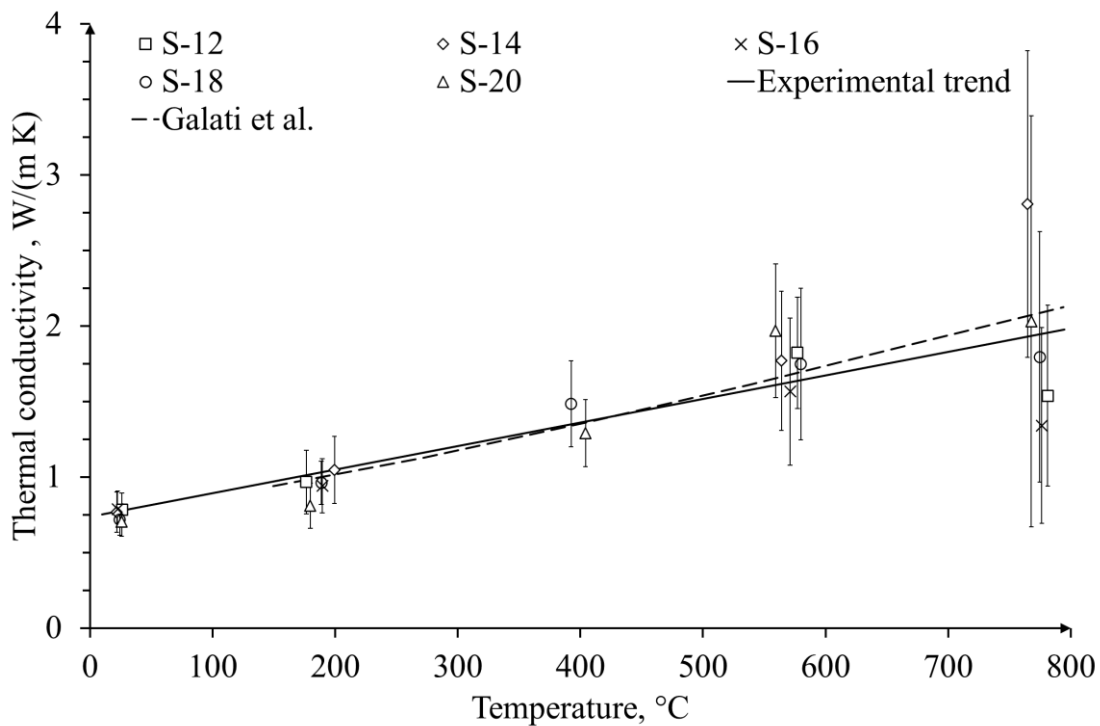


Fig. 3. Experimental thermal conductivity of sintered Ti6Al4V and comparison with the analytic data reported in Galati et al.[9].

4. Conclusion

This study characterised the Ti6Al4V powder used in EB-PBF, in the sintered state. The designed sample was a shell, which enclosed a certain thickness of sintered powder in vacuum. The most remarkable result is that the thermal conductivity of the sintered powder, which can be

assimilated to a porous material, does not vary with thickness. The dependency of the thermal conductivity on the temperature is linear. The proposed methodology to acquire the thermal conductivity of the sintered powder provides extremely important information for improving the accuracy of the modelling input and more in general to understand the physics beyond the process.

References

- [1] Galati M, Iuliano L, A literature review of powder-based electron beam melting focusing on numerical simulations. *Addit. Manuf.* 2018. 19: 1–20.
- [2] Galati M, Snis A, Iuliano L, Powder bed properties modelling and 3D thermo-mechanical simulation of the additive manufacturing Electron Beam Melting process. *Addit. Manuf.* 2019. 30.
- [3] Körner C, Attar E, Heintl P, Korner C, Attar E, Heintl P, Mesoscopic simulation of selective beam melting processes. *J. Mater. Process. Technol.* 2011. 211(6): 978–87.
- [4] Gong X, Anderson T, Chou K, Review on powder-based electron beam additive manufacturing technology. *ASME/ISCIE 2012 International Symposium on Flexible Automation*, vol. 1. American Society of Mechanical Engineers p. 507–15.
- [5] Gong X, Chou K, Characterization of sintered Ti-6Al-4V powders in electron beam additive manufacturing. *ASME 2013 International Manufacturing Science and Engineering Conference Collocated with the 41st North American Manufacturing Research Conference, MSEC 2013*, vol. 1. American Society of Mechanical Engineers Digital Collection.
- [6] Galati M, Snis A, Iuliano L, Experimental validation of a numerical thermal model of the EBM process for Ti6Al4V. *Comput. Math. with Appl.* 2018. 78(7): 2417–27.
- [7] Gong X, Cheng B, Price S, Chou K, Powder-bed electron-beam-melting additive manufacturing: powder characterization, process simulation and metrology. *Proceedings of the ASME District F Early Career Technical Conference*, p. 59–66.
- [8] Shen N, Chou K, Simulations of Thermo-Mechanical Characteristics in Electron Beam Additive Manufacturing. *ASME Int. Mech. Eng. Congr. Expo. Proc.* 2013. 3(PARTS A, B, AND C): 67–74.
- [9] Galati M, Iuliano L, Salmi A, Atzeni E, Modelling energy source and powder properties for the development of a thermal FE model of the EBM additive manufacturing process. *Addit. Manuf.* 2017. 14: 49–59.
- [10] Grose J, Cullinan M, Dibua OG, Behera D, Foong CS, Simulation and Characterization of Nanoparticle Thermal Conductivity for a Microscale Selective Laser Sintering System. *Proc. ASME 2021 16th Int. Manuf. Sci. Eng. Conf. MSEC 2021*. 2021. 2.
- [11] Wei LC, Ehrlich LE, Powell-Palm MJ, Montgomery C, Beuth J, Malen JA, Thermal conductivity of metal powders for powder bed additive manufacturing. *Addit. Manuf.* 2018. 21: 201–8.
- [12] Zhang S, Lane B, Whiting J, Chou K, On thermal properties of metallic powder in laser powder bed fusion additive manufacturing. *J. Manuf. Process.* 2019. 47: 382–92.
- [13] Gong X, Cheng B, Price S, Chou K, Powder-bed electron-beam-melting additive manufacturing: powder characterization, process simulation and metrology. *Early Career Tech. Conf. Birmingham, AL*. 2013. (November 2013): 55–66.
- [14] Neira Arce A, Thermal Modeling and Simulation of Electron Beam Melting for Rapid Prototyping on Ti6Al4V Alloys. 2012.
- [15] Smith CJ, Tammam-Williams S, Hernandez-Nava E, Todd I, Tailoring the thermal conductivity of the powder bed in Electron Beam Melting (EBM) Additive Manufacturing. *Sci. Rep.* 2017. 7(1): 1–8.
- [16] Leung CLA, Tosi R, Muzangaza E, Nonni S, Withers PJ, Lee PD, Effect of preheating on the thermal, microstructural and mechanical properties of selective electron beam melted Ti-6Al-4V components. *Mater. Des.* 2019. 174: 107792.
- [17] Cooper SJ, Bertel A, Shearing PR, Kilner JA, Brandon NP, TauFactor: An open-source application for calculating tortuosity factors from tomographic data. *SoftwareX*. 2016. 5.
- [18] Galati M, Rizza G, Defanti S, Denti L, Surface roughness prediction model for Electron Beam Melting (EBM) processing Ti6Al4V. *Precis. Eng.* 2021. 69.
- [19] Parker WJ, Jenkins RJ, Butler CP, Abbott GL, Flash method of determining thermal diffusivity, heat capacity, and thermal conductivity. *J. Appl. Phys.* 1961. 32(9).
- [20] Cape JA, Lehman GW, Temperature and finite pulse-time effects in the flash method for measuring thermal diffusivity. *J. Appl. Phys.* 1963. 34(7).
- [21] Cowan RD, Pulse method of measuring thermal diffusivity at high temperatures. *J. Appl. Phys.* 1963. 34(4).
- [22] Lee HL, Thermal Diffusivity in Layered and Dispersed Composites. Purdue University, Lafayette, IN, USA, 1975.
- [23] Sweet JN, Data analysis methods for flash thermal diffusivity experiments. Albuquerque, NM, and Livermore, CA (United States).
- [24] Larson KB, Koyama K, Measurement by the flash method of thermal diffusivity, heat capacity, and thermal conductivity in two-layer composite samples. *J. Appl. Phys.* 1968. 39(9).
- [25] Hartmann J, Nilsson O, Fricke J, Thermal Diffusivity Measurements on Two-Layered and Three-Layered Systems with the Laser-Flash Method. *High Temp. High Press.* 1993. .
- [26] Hobbie EK, De Reggi AS, Laser-pulse technique for measuring the thermal diffusivity of substrate-supported polymer films. *Rev. Sci. Instrum.* 1999. 70(11).
- [27] Watt DA, Theory of thermal diffusivity by pulse technique. *Br. J. Appl. Phys.* 1966. 17(2).
- [28] Müller B, Renz U, Development of a fast fiber-optic two-color pyrometer for the temperature measurement of surfaces with varying emissivities. *Rev. Sci. Instrum.* 2001. 72(8).
- [29] Boivineau M, Cagran C, Doytier D, Eyraud V, Nadal M-H, Wilthan B, et al., Thermophysical properties of solid and liquid Ti-6Al-4V (TA6V) alloy. *Int. J. Thermophys.* 2006. 27(2): 507–29.
- [30] Shapiro M, Dudko V, Royzen V, Krichevets Y, Lekhtmakher S, Grozubinsky V, et al., Characterization of Powder Beds by Thermal Conductivity: Effect of Gas Pressure on the Thermal Resistance of Particle Contact Points. *Particle and Particle Systems Characterization*, vol. 21.
- [31] Tolochko NK, Arshinov MK, Gusarov A V, Titov VI, Laoui T, Froyen L, Mechanisms of selective laser sintering and heat transfer in Ti powder. *Rapid Prototyp. J.* 2003. 9(5): 314–26.